COBEM 2023 27TH INTERNATIONAL CONGRESS OF MECHANICAL ENGINEERING

ABCM Brazilian Society of Mechanical Sciences and Engineering
27th ABCM International Congress of Mechanical Engineering
December 04-08, 2023, Florianópolis-SC, Brazil

COB-2023-0644
FLUID-STRUCTURE INTERACTION IN INDUSTRIAL APPLICATION USING THE FINITE ELEMENT - IMMERSED BOUNDARY APPROACH

Freddy Alejandro Portillo Morales
alejandro@ufu.br
Aristeu da Silveira Neto
aristeus@ufu.br
Aldemir Aparecido Cavallini Jr.
aacjunior@ufu.br
Leandro Jose Lemes Stival
leandrostival@gmail.com

Federal University of Uberlândia (UFU), 2121 Av. João Naves de Ávila, Uberlândia, MG, Brazil

Abstract. *Fluid-structure interaction (FSI) is a complex phenomenon that occurs when a fluid flow interact with a flexible structure. There are so many ways to simulate numerically that kind of physical problems. This article discusses the numerical implementation of simulation routines for FSI analysis using a coupling of Finite Element Method (FEM), Immersed Boundary Method (IBM) and Finite Volume Method (FVM). This approach allows to solve FSI problems with a low computational cost when compared with ALE (Arbitrary Lagrangian Eulerian) methods, because it can be solved using structured meshes for the fluid solver. The computational implementations were made into MFSim, code developed by the Fluid Mechanics Laboratory (MFLab) of University of Uberlandia in partnership with Petrobras. The FEM is a numerical method that discretizes the domain into small elements and solve the governing equations for each one of these elements considering their respective connections where the solution is approximated by polynomial functions, allowing to solve different kind of physical phenomena as solid mechanics, fluid mechanics, electromagnetism, electrical circuits, etc. The IBM is a technique that enables the representation of the solid geometry within the fluid domain by imposing a force on the fluid through a Lagrangian force term. Finally, the FVM is a numerical method that discretize the domain into small control volumes where the conservation equations are solved. The article presents results of FSI simulations of a flexible vertical flap with a perpendicular air flow. The results demonstrate the effectiveness of the coupling approach, as well as the importance of accurate modeling of FSI problems. The simulations shows the deformation of the structure due to the interaction of the fluid in time and how the presence of the structure affects the flow. This paper demonstrates the application of FSI analysis in an industrial context, specifically focusing on a pipeline system within a Fluid Catalytic Cracking Unit used in the oil and gas industry. The analysis involves the use of butterfly valves positioned at different angles of opening. The fluid flow in the system is considered compressible, with properties that vary.*

Keywords: *Fluid-Structure Interaction, Finite Element Method, Finite Volume Method, Immersed Boundary Method, MFSim*

1. INTRODUCTION

The phenomenon of fluid-structure interaction (FSI) involves the interaction between one or more solid bodies and the external and/or internal flow of a fluid. FSI problems arise in various natural and engineering scenarios. In nature, examples include the flapping of insect wings, airflow between trees, and blood flow through veins and arteries in the human body. In engineering, FSI analysis plays a critical role in the mechanical design of airplanes and rockets, the construction of bridges and tall structures like skyscrapers, offshore oil platforms, and even the design of wind turbines, among other applications.

Computational simulations of FSI problems are inherently complex due to the simultaneous solution of fluid dynamics and structural dynamics. The coupling of these physical subsystems can be achieved through monolithic or partitioned approaches. In the monolithic approach, a single system of equations is solved, incorporating both fluid dynamics and structural analysis. Conversely, the partitioned approach involves employing distinct methods to solve each physics domain separately and then coupling them together.

The use of computational numerical tools has experienced significant growth in recent decades, primarily driven by the ability to simulate increasingly larger problems that are challenging to analyze experimentally in laboratories. In some cases, the size or complexity of the problem, or the inability to control variables for accurate replication, makes experimental analysis impractical. However, this does not imply the disregard of experimental material analyses, as they

remain crucial for validating computational simulations. Thus, both virtual and material experiments serve complementary roles and engage in constant interaction.

MFSim is a multi-physics simulation software designed to analyze compressible and incompressible fluid dynamics, multiphase flows, combustion, corrosion, and fluid-structure interaction problems. Developed by the Fluid Mechanics Laboratory (MFLab) at the Federal University of Uberlândia (UFU) in collaboration with Petrobras, the software has been utilized in numerous industrial application projects and academic research endeavors.

In this work, the partitioned approach was adopted, using FEM to solve the structural subsystem and the FVM to solve the fluid subsystem. The coupling between the two methods is performed through IBM Peskin (1972); Wang *et al.* (2008), which works as an interface between the two subsystems mentioned above.

This paper details a research study in which computational Fluid-Structure Interaction (FSI) simulations were performed to investigate a particular issue related to a pipeline featuring an internal layer of refractory concrete. The control of mass flow rate in the pipeline is achieved through the operation of a butterfly valve and a gate valve, both of which are integral components of a Fluid Catalytic Cracking Unit (FCCU) commonly utilized in the oil and gas industry.

The primary aim of this study is to examine the flow-induced vibrations under various valve opening configurations. In certain instances, such vibrations can lead to the separation or detachment of the internal concrete layer within the pipeline.

2. DIFFERENTIAL MATHEMATICAL MODEL

2.1 Fluid subsystem

The equations for mass balance (Eq. 1), linear momentum balance (Eq. 2) and thermal energy balance (Eq. 3) for a compressible flow are written below in divergent form and with Einstein notation, respectively.

$$\frac{\partial \rho}{\partial t} + \frac{\partial (\rho u_i)}{\partial x_i} = 0, \tag{1}$$

$$\frac{\partial (\rho u_i)}{\partial t} + \frac{\partial (\rho u_i u_j)}{\partial x_j} = -\frac{\partial p}{\partial x_i} + \frac{\partial \tau_{ij}}{\partial x_j} + \rho f_i, \tag{2}$$

$$\frac{\partial (\rho c_p T)}{\partial t} + \frac{\partial (\rho c_p T u_j)}{\partial x_j} = \frac{\partial}{\partial x_j}\left(k \frac{\partial T}{\partial x_j}\right) + \Phi + \frac{\partial p}{\partial t} + u_j \frac{\partial p}{\partial x_j}, \tag{3}$$

where i and j vary from 1 to 3, ρ is the mass density, t is the temporal variable, u_i is a component of the velocity vector $\vec{u}$, p is the pressure, τ is the viscous stress tensor (Eq. 4), f_i is the source term that represents the components of the force vector acting on the fluid, T is the temperature, k is the thermal conductivity, c_p is the specific heat at constant pressure and Φ, which is the viscous energy transformation function, given by Eq. 5.

$$\tau_{ij} = \mu\left(\frac{\partial u_i}{\partial x_j} + \frac{\partial u_j}{\partial x_i} - \frac{2}{3}\frac{\partial u_k}{\partial x_k}\delta_{ij}\right), \tag{4}$$

$$\Phi = 2\mu(S_{ij}S_{ij} - \frac{1}{3}S_{kk}S_{pp}). \tag{5}$$

In Eq. 4, δ_{ij} is the Kronecker delta, given by Eq. 6, μ is the dynamic viscosity. In the Eq. 5 , S_{ij} is the strain rate tensor, given by $S_{ij} = \frac{1}{2}\left(\frac{\partial u_i}{\partial x_j} + \frac{\partial u_j}{\partial x_i}\right)$.

$$\delta_{ij} = \begin{cases} 1; & \text{for } i = j \\ 0; & \text{for } i \neq j \end{cases} \tag{6}$$

To take into account the variation of mass density as a function of temperature and pressure, the equation of state given by Eq. 7 is used.

$$\rho = \frac{p + p_\infty}{RT}, \tag{7}$$

where p_∞ is given by $p_\infty = \gamma \cdot p_0$, where p_0 is a characteristic parameter of the material (for an ideal gas, $P_0 = 0$) and $\gamma = \frac{c_p}{c_v}$, c_v is the specific heat at constant volume.

2.2 Structural subsystem

To derive the motion equations for mass-spring systems, the principle of minimum action is used, using a Hamiltonian approach. In the Hamiltonian principle, the variational operator (δ) is used applied to the Lagrangian of a system (Eq. 8).

$$\delta \int_{t_1}^{t_2} L \, dt = 0, \tag{8}$$

Where the Lagrangian (L) is the difference between the kinetic energy (K) and the total potential energy (Π) of the system. Substituting the concept of Lagrangian in Eq. 8, we have:

$$\delta \int_{t_1}^{t_2} (K - \Pi) \, dt = 0. \tag{9}$$

The total potential energy can be deduced using the principles of minimum potential energy and virtual work. The total potential energy is the difference between the internal potential energy and the external potential energy, in other words, the internal deformation energy (U) and the external virtual work produced by external forces (W_e). Therefore, $\Pi = U - W_e$. Substituting in Eq. 9 we have that:

$$\delta \int_{t_1}^{t_2} (W_e - U + K) \, dt = 0. \tag{10}$$

The field equations for solid mechanics are governed by equilibrium behavior (moment equilibrium), constitutive equations of the strain-displacement relationships, boundary conditions, and initial conditions Zienkiewicz *et al.* (2013).

The equilibrium equations are given by:

$$\begin{aligned}
&\frac{\partial \sigma_x}{\partial x} + \frac{\partial \tau_{yx}}{\partial y} + \frac{\partial \tau_{zx}}{\partial z} + f_x = \rho \frac{\partial^2 u}{\partial t^2}, \\
&\frac{\partial \tau_{xy}}{\partial x} + \frac{\partial \sigma_y}{\partial y} + \frac{\partial \tau_{zy}}{\partial z} + f_y = \rho \frac{\partial^2 v}{\partial t^2}, \\
&\frac{\partial \tau_{xz}}{\partial x} + \frac{\partial \tau_{yz}}{\partial y} + \frac{\partial \sigma_z}{\partial z} + f_z = \rho \frac{\partial^2 w}{\partial t^2},
\end{aligned} \tag{11}$$

where the Cauchy's stress tensor (σ) is given by:

$$\sigma = \begin{bmatrix} \sigma_{11} & \sigma_{12} & \sigma_{13} \\ \sigma_{21} & \sigma_{22} & \sigma_{23} \\ \sigma_{31} & \sigma_{32} & \sigma_{33} \end{bmatrix} = \begin{bmatrix} \sigma_x & \tau_{xy} & \tau_{xz} \\ \tau_{yx} & \sigma_y & \tau_{yz} \\ \tau_{zx} & \tau_{zy} & \sigma_z \end{bmatrix}. \tag{12}$$

The linear moment equilibrium equations can be rewritten in Einstein notation as follows:

$$\frac{\partial \sigma_{ij}}{\partial x_j} + f_i = \rho \, \frac{\partial^2 u_i}{\partial t^2}, \tag{13}$$

where $i, j = 1, 2, 3$, ρ is the mass density, $\ddot{u}_i$ is the second derivative of displacement, and f_i is a component of the external force vector $\vec{f}$. For elastic materials, the structural stresses follow Hooke's law as shown below:

$$\sigma_{ij} = \lambda \delta_{ij} \varepsilon_{ll} + 2G \varepsilon_{ij}, \tag{14}$$

$$\varepsilon_{ij} = \frac{1}{2} \Big(\frac{\partial u_i}{\partial x_j} + \frac{\partial u_j}{\partial x_i} \Big), \tag{15}$$

where δ_{ij} is the Kronecker delta given by Eq. 6, σ_{ij} is the stress tensor, ε_{ij} is the strain tensor, and λ and G are the Lamé constants. Assuming homogeneous and isotropic material, they are defined as:

$$G = \frac{E}{2(1+\nu)}, \tag{16}$$

$$\lambda = \frac{E\nu}{(1+\nu)(1-2\nu)}, \tag{17}$$

where E and ν are the Young's modulus and Poisson's ratio, respectively.

By using the Principle of Virtual Work (Eq. 18), there is an equality between the virtual work done by external forces and the virtual work due to internal stresses.

$$\delta\Pi = \delta U - \delta W_e = 0 \tag{18}$$

$$\int_V \sigma_{ij}\, \delta\varepsilon_{ij}\, dV - \int_V f_i \delta u_i dV = 0. \tag{19}$$

The kinetic energy (Eq. 20) is calculated as the integral over the volume of the mass density multiplied by the square of the velocity.

$$\delta K = \frac{1}{2}\int_V \rho \frac{\partial(u_i)}{\partial t}\, \frac{\partial(\delta u_i)}{\partial t} dV. \tag{20}$$

By substituting Eqs. 19 and 20 into Eq. 10 and applying the fundamental theorem of variational calculus, we obtain the equation of motion for a system, presented below in matrix form for simplicity:

$$\int_{t_1}^{t_2} ([M]\{\ddot{u}\} + [K]\{u\})dt = \int_{t_1}^{t_2} \{f\}dt. \tag{21}$$

Where $[M]$ is the mass matrix of the system, $[K]$ represents the stiffness matrix, $\{f\}$ is the vector of external forces, $\{u\}$ is the displacement vector, and $\{\ddot{u}\}$ is the acceleration vector.

The discretized finite element equations are obtained by evaluating the kinetic energy and elastic potential energy. In this work, the structure is treated with solid elements, whose method is described in Morales *et al.* (2022).

2.3 FSI coupling

The fluid-structure coupling, in partitioned way, is possible by solving the fluid and structural subsystems using FVM and FEM methods, and coupled through the immersed boundary method. This coupling can be strong or weak. The immersed frontier method allows the determination of those produced by the flow under the structure, which would be the source term of the momentum conservation equation (Navier-Stokes).

For the implementation of the immersed boundary method, a complementary STL (Standard Triangle Language) mesh is needed, the size of the elements of this mesh is calculated as a function of the size of the cells of the highest level of refinement. To carry out the transmission of forces, each element of the FEM mesh searches around it and finds the points of the STL mesh with which they are in contact, after identifying the points of the lagrangian mesh, the forces related to such points are interpolated and distributed in the respective nodes of the FEM mesh.

The algorithm used in the weak coupling of FSI is presented below in Algorithm 1.

3. COMPUTATIONAL FRAMEWORK

The present work utilizes the computational framework known as MFSim, which was developed at the Fluid Mechanics Laboratory at the Federal University of Uberlândia, Brazil. This platform, initially introduced by Villar Villar (2007), has undergone continuous development over the years, evolving into a versatile code with a multidisciplinary focus.

Currently, MFSim offers the capability to simulate various 3D problems, including turbulent flow Vedovoto *et al.* (2015); Damasceno *et al.* (2015), fluid-structure interaction Ribeiro Neto *et al.* (2019); Souza *et al.* (2022); Stival *et al.* (2022), multi-phase phenomena Pivello *et al.* (2014); Barbi *et al.* (2018); Pinheiro *et al.* (2019, 2021), gas-solid and gas-liquid flows Santos (2019), reactive processes Damasceno *et al.* (2018); Castro *et al.* (2021), and also incorporates LES approaches with both isotropic and anisotropic modeling.

In recent times, MFSim was employed to assess hypersaline solutions disposal operations, with a focus on complying with local environmental regulations to minimize the impact on marine ecosystems Mota *et al.* (2023).

Algorithm 1 Weak FSI coupling

while do$(t < t_{max}$ and $n < n_{max})$
$t^{n+1} = t^n + \Delta t$
$(\dots)$ Solve fluid subsystem
$F_{flow}^{n+1} = F_{flow}\left(v^*(\vec{x}), \begin{Bmatrix} u(\vec{x}_k) \\ \dot{u}(\vec{x}_k) \end{Bmatrix}^n\right)$
$\begin{bmatrix} u(\vec{x}_k) \\ \dot{u}(\vec{x}_k) \end{bmatrix}^{n+1}$= PV $\left(\, t^n, \Delta t, F_{flow}^{n+1}\right)$ Pressure-velocity coupling
$(\dots)$ Solve structure subsystem
$n = n + 1$

4. RESULTS AND DISCUSSION

The problem proposed to be solved was about the FSI analysis of a pipeline featuring a butterfly valve, which constitutes a crucial component within fluid catalytic cracking units (FCCU) in the oil and gas industry.

This specific segment (pipeline) of the unit serves the purpose of transporting the combustion gases generated during the petroleum refining process. The FCCU piping system comprises two distinct layers of materials: an inner layer constructed from refractory concrete and an outer layer comprised of steel piping. These two layers are interconnected through the use of metal clamps.

The operational parameters of the FCCU, including factors like mass flow rate, downstream pressure, and upstream pressure, are contingent upon the manipulation of two primary valves. These valves are identified as the 'Main' valve, represented as a butterfly valve, and the 'Slide' valve, which is a gate valve. It's important to note that the 'Slide' valve, positioned at the outlet of the domain, is not explicitly represented in the physical model. Nevertheless, it plays a pivotal role in regulating the system's mass flow rate. The initial gas properties are presented in Table 1.

Table 1. Combustion gases properties

Property	
Fluid density, ρ_f	$0.781845\ \frac{kg}{m^3}$
Dynamic viscosity, μ_f	$3.84252\ Pa \cdot s$
Specific heat, C_p	$1261.476\ \frac{J}{kg \cdot K}$
Thermal conductivity, κ	$0.0676\ \frac{W}{m \cdot K}$
Temperature, T	$911\ K$

The FEM structural model consisted of coupling the steel and concrete layers. The properties used for each material are listed in Table 2. The mesh used is shown in Figure 1. The mesh consists of a total of 29,400 hexahedral elements, with a total of 42,900 nodes.

Table 3 displays the results regarding the initial 14 vibration modes of the pipe, as investigated in this study. These findings account for the presence of a rigid node-to-node coupling between the steel and concrete layers of the pipe, as detailed in the research.

As a summary, in Tab. 4, the general parameters of the performed simulations are listed.

Table 2. Properties of structural materials

Steel	
Specific mass	$\rho_s = 7829\, kg/m^3$
Young's module	$E_s = 206.9\, GPa$
Poisson's ratio	$\nu_s = 0.288$
Refractory concrete	
Specific mass	$\rho_c = 1750\, kg/m^3$
Young's module	$E_c = 9.54\, GPa$
Poisson's ratio	$\nu_c = 0.30$

Figure 1. FEM mesh and boundary conditions for the structure.

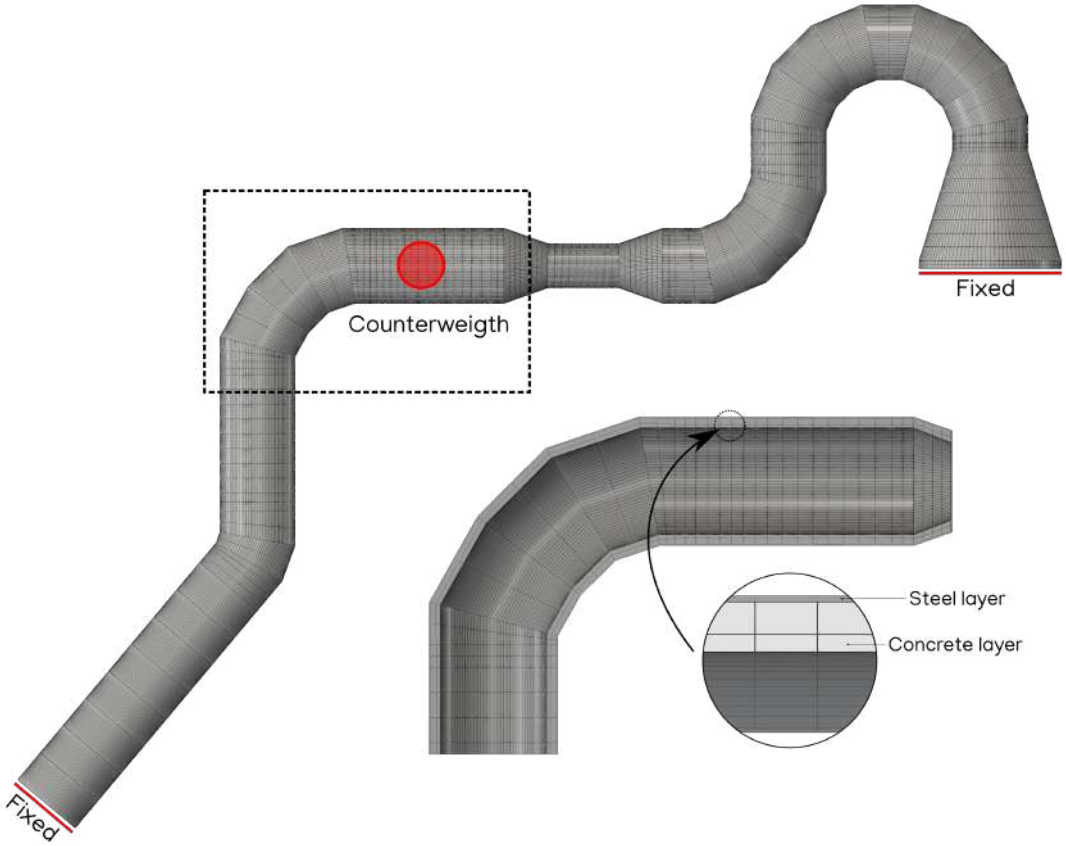

Table 3. Natural frequencies from modal analysis for the structure.

Mode of vibration	Natural frequency [Hz]	Mode of vibration	Natural frequency [Hz]
1	5.475	8	24.233
2	5.915	9	29.599
3	11.023	10	30.725
4	13.912	11	57.402
5	21.557	12	58.614
6	22.615	13	76.441
7	23.520	14	80.778

In Figure 2, the simulation results for the case 00m100s are presented. On the left, the iso-surfaces of the Q criterion are shown, colored according to the flow velocity magnitude. On the right, the magnitude of the structural displacement for the same moment in time is displayed.

Table 4. Computational simulation setup

Parameter	
Processor	AMD Epyc 7452
Number of processors per job	64
Number of fluid cells	9 999 080
Number of physical levels	5
Cells size on *ltop*	$18.75\,mm$
Number of IB elements	664 328
Number of FEM elements	29 400
Number of DOFs for structure subsystem	128 700
Number of modes calculated	20
Cells distribution on *lbot*	$80 \times 40 \times 20$
Pressure-velocity coupling scheme	PISO
Temporal discretization method	MCNAB
Advective term discretization model	TVD_SUPERBEE
Turbulence closure model	LES - Smagorinsky
Smagorinsky constant	0.18
Processors distribution	$8 \times 4 \times 2$
Physical time simulated	$2.00s$

Figure 2. On the left, Iso surfaces of the Q criterion colored by the velocity magnitude, and on the right, the magnitude of the structural displacement with 2 seconds of physical simulation.

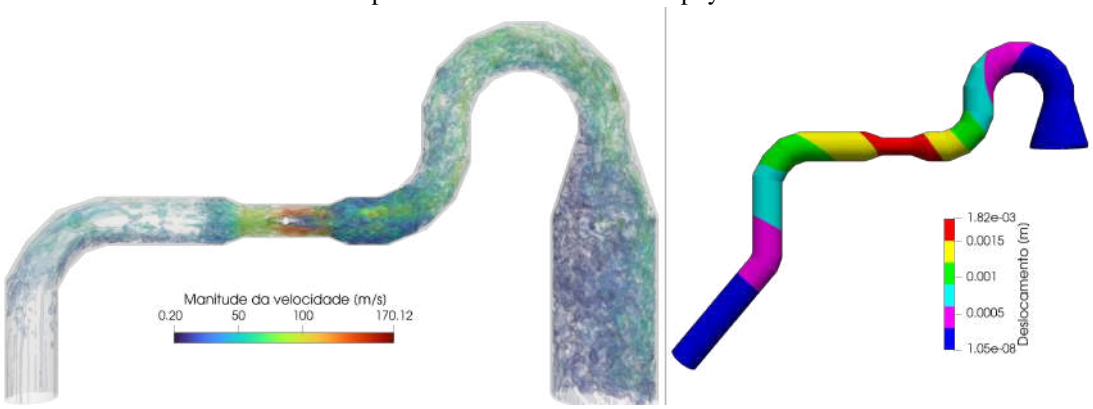

00m100s
Fonte: elaborada pelo autor

To effectively manage the substantial volume of data generated in our study, we have chosen to employ the Response Surface Methodology (RSM), a method originally introduced by Box and Draper (1959). RSM is a valuable approach for investigating the relationships between multiple input variables and response variables, and it is particularly useful for modeling and optimizing complex processes.

In the context of our research, we designated the 'Main' and 'Slide' valve openings as input variables, while the maximum displacement in the structure was considered as the output variable. The application of RSM provides a more accessible means of interpreting the system's behavior with respect to these defined variables.

Figures 3 and 4 exhibit the outcomes obtained by applying RSM to the computational probes located within the region displaying the highest vibration amplitude. These visual representations depict the response surfaces generated through statistical models using machine learning, offering a vivid illustration of the connections between the input variables and the output variable. To gauge the precision of the response surface, we include two parameters: RMSE (Root Mean Square Error) and R^2 (Coefficient of Determination).

Figure 3. Surface response of the mean of displacement magnitude at node 22401 (upstream to the main valve) for all the configurations simulated.

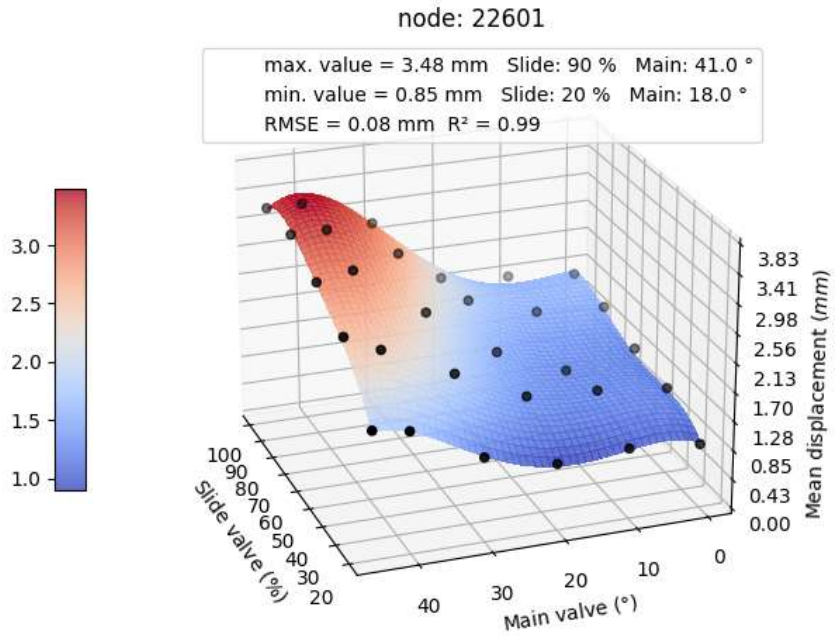

Figure 4. Surface response of the mean of displacement magnitude at node 24801 (downstream to the main valve) for all the configurations simulated.

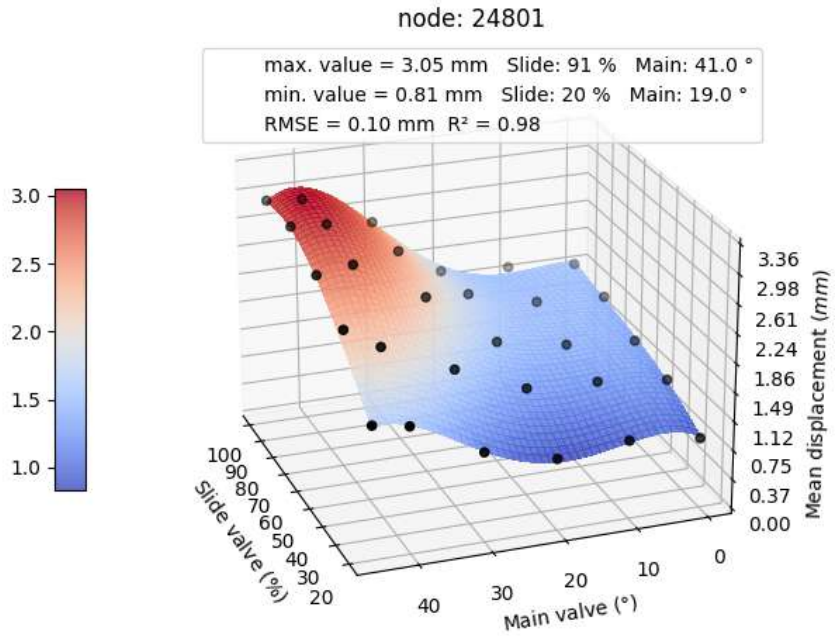

The results, from the RSM, indicate that the highest mean displacement magnitude value occurs when the 'Main' valve is open at 41° and the 'Slide' valve is at 91%.

On the other hand, the results showed that the lowest mean displacement magnitude occurs when the 'Main' valve is open at 19° and the 'Slide' valve is at 20%.

Subsequently, we present the spectra results derived from the probes situated within the fluid domain. This step is taken to gain deeper insights into the findings previously illustrated through the generated response surfaces. The probes under analysis were strategically positioned both upstream and downstream of the Main valve, as visually indicated in Fig. 5. Also, the results for velocity and pressure for these two probes are presented from Fig. 6 to Fig. 8.

Figure 5. Mach number of the flow and probes location for upstream (A) and downstream (B) to the Main valve for 45m100s case.

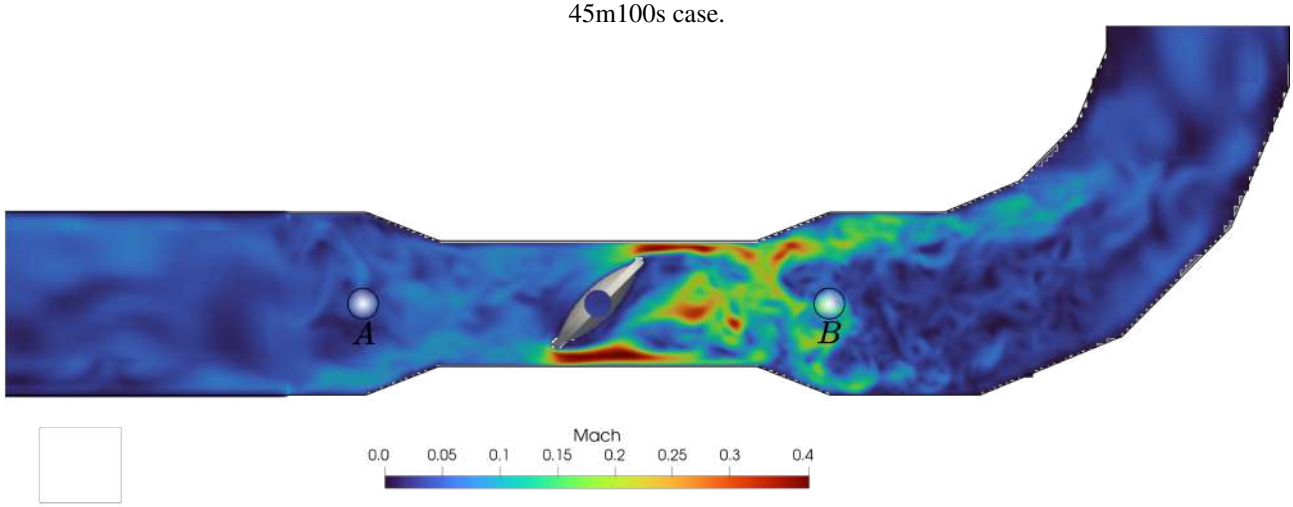

Figure 6. Velocity magnitude at upstream (A) and downstream (B) to the Main valve for 45m100s.

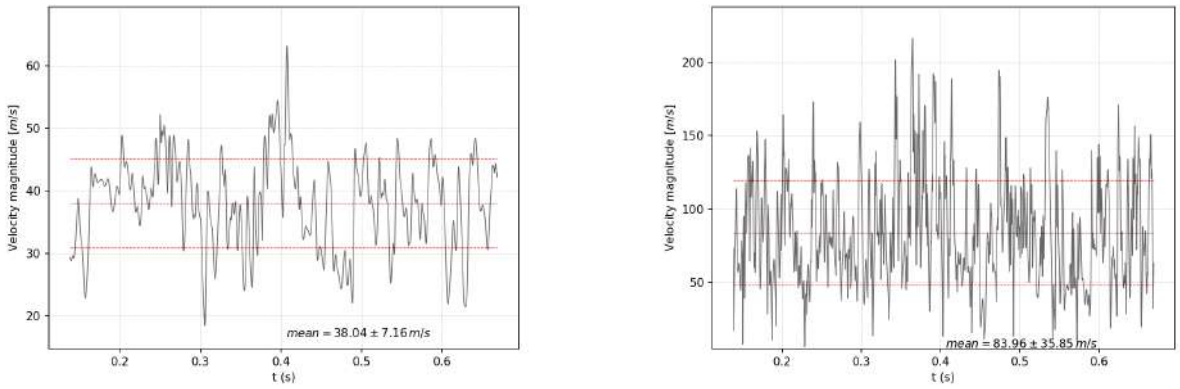

A B

Figure 7. Pressure at upstream (A) and downstream (B) to the Main valve for 45m100s.

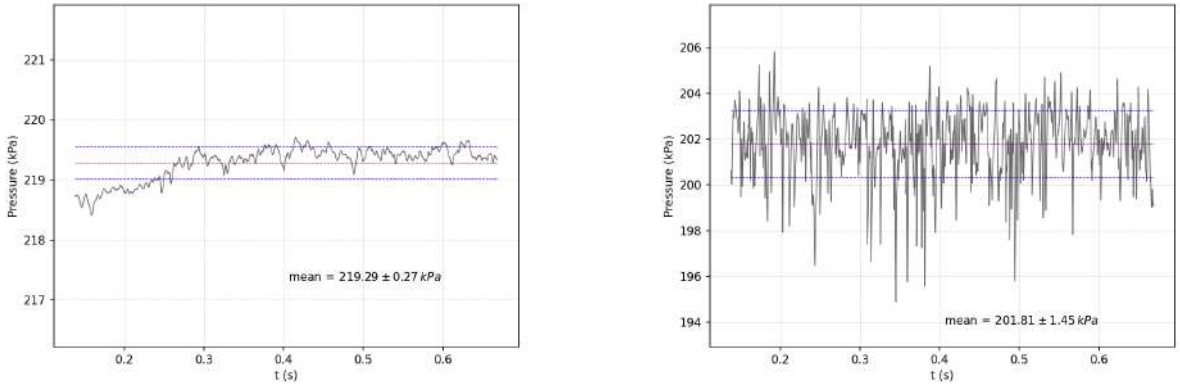

A B

Figure 8. Turbulent kinetic energy spectrum at upstream (A) and downstream (B) to the Main valve for 45m100s.

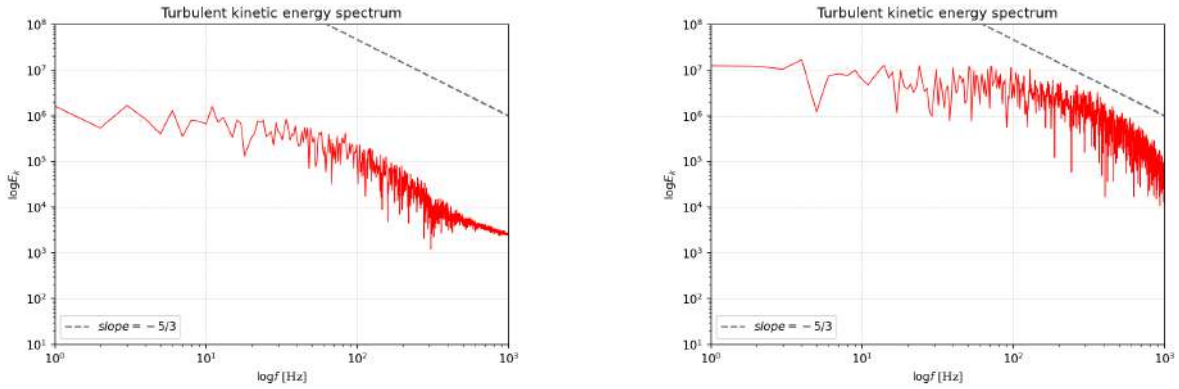

A B

The intricate nonlinearities intrinsic to the problem pose challenges to its predictability. Notably, the downstream region exhibits more pronounced pressure fluctuations and heightened turbulent kinetic energy. However, it is imperative to acknowledge that the structural integrity remains a cohesive entity, intricately interwoven and subject to fluid dynamic forces that span the entire domain. Consequently, asserting that the most significant structural displacement would invariably manifest exclusively downstream of the valve would be an oversimplification.

5. CONCLUSIONS

An assessment of the fluid-structure interaction within a compressible flow problem was conducted by implementing a Finite Element - Immersed Boundary approach. The utilization of MFSim, which incorporates a partitioned approach, allowed for the seamless integration of various computational methods for each subsystem. Adaptive meshing techniques were applied throughout the simulations. As a result, the natural frequencies of the structure, accounting for the influences of the two-layer materials, were accurately determined.

The results from the response surface analysis reveal that the highest average displacement magnitude in the upstream structural region of the Main valve is achieved when it is set to an opening angle of 41°, in conjunction with the Slide valve being at 90%.

Moreover, the findings also indicate that the smallest average displacement magnitude in the same region is attained when the Main valve is operated with an opening angle of 18°, and the Slide valve is set at 20%.

6. ACKNOWLEDGEMENTS

The authors gratefully acknowledge technical and financial support from CAPES, FAPEMIG, CNPq, and Petróleo Brasileiro S.A. (Petrobras). Thanks to FURNAS and the ANEEL R&D Program for the financial support. The authors are also grateful to the Graduate Program in Mechanical Engineering at the Federal University of Uberlândia.

7. REFERENCES

Barbi, F., Pivello, M.R., Villar, M.M., Serfaty, R., Roma, A.M. and Silveira Neto, A.d., 2018. "Numerical experiments of ascending bubbles for fluid dynamic force calculations". *Journal of the Brazilian Society of Mechanical Sciences and Engineering*, Vol. 40, No. 11, p. 519. ISSN 1806-3691. doi:10.1007/s40430-018-1435-7.

Box, G.E. and Draper, N.R., 1959. "A basis for the selection of a response surface design". *Journal of the American Statistical Association*, Vol. 54, pp. 622–654. ISSN 1537274X. doi:10.1080/01621459.1959.10501525.

Castro, L.P.d., Pinheiro, A.P., Vilela, V., Magalhães, G.M., Serfaty, R. and Vedovotto, J.M., 2021. "Implementation of a hybrid lagrangian filtered density function–large eddy simulation methodology in a dynamic adaptive mesh refinement environment". *Physics of Fluids*, Vol. 33, No. 4, p. 045126. doi:10.1063/5.0045873.

Damasceno, M., Vedovoto, J. and Silveira-Neto, A., 2015. "Turbulent inlet conditions modeling using large-eddy simulations". *CMES - Computer Modeling in Engineering and Sciences*, Vol. 104, pp. 105–132.

Damasceno, M.M.R., de Freitas Santos, J.G. and Vedovoto, J.M., 2018. "Simulation of turbulent reactive flows using a fdf methodology – advances in particle density control for normalized variables". *Computers & Fluids*, Vol. 170, pp. 128 – 140. ISSN 0045-7930. doi:https://doi.org/10.1016/j.compfluid.2018.05.004.

Morales, F., Silveira-Neto, A., Cavallini Jr, A., Preta, R. and Chiumento, V., 2022. "Fluid-structure interaction for turbulent incompressible flow over a cylinder-plate system". *13th Spring School on Transition and Turbulence*. doi:

10.26678/ABCM.EPTT2022.EPT22-0020.

Mota, P.H.A., Vedovotto, J.M. and Aristeu, S.N., 2023. "Assessment of critical brine disposal operations conditions by cfd modeling and a kriging metamodel". *Environmental Fluid Mechanics*, Vol. 167, pp. 1573–1510. doi:10.1007/s10652-023-09911-7.

Peskin, C.S., 1972. "Flow patterns around heart valves: A numerical method". *Journal of Computational Physics*, Vol. 10, pp. 252–271.

Pinheiro, A.P., Rybdylova, O., Zubrilin, I.A., Sazhin, S.S., Sacomano Filho, F.L. and Vedovotto, J.M., 2021. "Modelling of aviation kerosene droplet heating and evaporation using complete fuel composition and surrogates". *Fuel*, Vol. 305, p. 121564. ISSN 0016-2361. doi:https://doi.org/10.1016/j.fuel.2021.121564. URL `https://www.sciencedirect.com/science/article/pii/S0016236121014459`.

Pinheiro, A.P., Vedovoto, J.M., da Silveira Neto, A. and van Wachem, B.G., 2019. "Ethanol droplet evaporation: Effects of ambient temperature, pressure and fuel vapor concentration". *International Journal of Heat and Mass Transfer*, Vol. 143, p. 118472. ISSN 0017-9310. doi:10.1016/j.ijheatmasstransfer.2019.118472. URL `https://www.sciencedirect.com/science/article/pii/S0017931019309214`.

Pivello, M., Villar, M., Serfaty, R., Roma, A. and Silveira-Neto, A., 2014. "A fully adaptive front tracking method for the simulation of two phase flows". *International Journal of Multiphase Flow*, Vol. 58, pp. 72–82. ISSN 0301-9322. doi:https://doi.org/10.1016/j.ijmultiphaseflow.2013.08.009.

Ribeiro Neto, H., Cavalini, A., Vedovoto, J.M., Silveira Neto, A. and Rade, D.A., 2019. "Influence of sea bed proximity on the vibration responses of a pipeline accounting for fluid-structure interaction". *Mechanical Systems and Signal Processing*, Vol. 114, pp. 224–238.

Santos, J.G.d.F., 2019. *Mathematical and computational modeling of gas-solid flows in dynamic adaptive mesh*. Master's thesis, Universidade Federal de Uberlândia, Uberlândia, Brazil.

Souza, P.R.C., Neto, H.R., Villar, M.M., Vedovotto, J.M., Cavalini, A.A. and Neto, A.S., 2022. "Multi-phase fluid–structure interaction using adaptive mesh refinement and immersed boundary method". *Journal of the Brazilian Society of Mechanical Sciences and Engineering*, Vol. 44. ISSN 18063691. doi:10.1007/s40430-022-03417-x.

Stival, L.J., Brinkerhoff, J.R., Vedovotto, J.M. and de Andrade, F.O., 2022. "Wake modeling and simulation of an experimental wind turbine using large eddy simulation coupled with immersed boundary method alongside a dynamic adaptive mesh refinement". *Energy Conversion and Management*, Vol. 268, p. 115938. ISSN 0196-8904. doi: https://doi.org/10.1016/j.enconman.2022.115938.

Vedovoto, J.M., Serfaty, R. and da Silveira-Neto, A., 2015. "Mathematical and numerical modeling of turbulent flows". *Anais da Academia Brasileira de Ciencias*, Vol. 87, pp. 1195–1232. ISSN 16782690. doi:10.1590/0001-3765201520140510.

Villar, M., 2007. *Análise numérica detalhada de escoamentos multifásicos bidimensionais*. Ph.D. thesis, Universidade Federal de Uberlândia, Uberlândia, Brazil.

Wang, Z., Fan, J. and Luo, K., 2008. "Combined multi-direct forcing and immersed boundary method for simulating flows with moving particles". *International Journal of Multiphase Flow*, Vol. 34, pp. 283–302.

Zienkiewicz, O.C., Taylor, R.L. and Nithiarasu, P., 2013. *The Finite Element Method for Fluid Dynamics: Seventh Edition*. ISBN 9781856176354. doi:10.1016/C2009-0-26328-8.

8. RESPONSIBILITY NOTICE

The author(s) is (are) solely responsible for the printed material included in this paper.